J. Fluid Mech. (2002), *vol.* 451, *pp.* 295–317.
DOI: 10.1017/S002211200100653X Printed in the United Kingdom

Transient motion of a confined stratified fluid induced simultaneously by sidewall thermal loading and vertical throughflow

By JUN SANG PARK[1] AND JAE MIN HYUN[2]†

[1]Department of Mechanical Engineering, Halla Institute of Technology, San 66, HeungUp, Wonju, Kangwondo 220-712, South Korea

[2]Department of Mechanical Engineering, Korea Advanced Institute of Science & Technology, 373-1 Kusong-Dong, Yusung-gu, Taejon 305-701, South Korea

(Received 6 August 2000 and in revised form 20 July 2001)

An analytical study is made of the transient adjustment process of an initially stationary, stably stratified fluid in a square container. The boundary walls are highly conducting. The overall Rayleigh number Ra is large. Flow is initiated by the simultaneous switch-on of a temperature increase (δT) at the vertical wall and a forced vertical throughflow ($Ra^{-1/4}\delta w$) at the horizontal walls. The principal characteristics are found by employing the matched asymptotic expansion method. The flow field is divided into the inviscid interior, vertical boundary layers and horizontal boundary layers and analyses are conducted for each region. The horizontal boundary layers are shown to be of double-layered structure, and explicit solutions are secured for these layers. Evolutionary patterns of velocity and temperature in the whole flow domain are illustrated. Both opposing ($\delta w/\delta T > 0$) and cooperating ($\delta w/\delta T < 0$) configurations are considered. The flow character in the opposing configuration can be classified into (*a*) a forced-convection dominant mode ($\delta w/\delta T > 1/\sqrt{2}$), (*b*) a buoyancy-convection-dominant mode ($0 < \delta w/\delta T < 1/\sqrt{2}$), and (*c*) a static mode ($\delta w/\delta T \approx 1/\sqrt{2}$). Global evolutionary processes are depicted, and physical rationalizations are provided.

1. Introduction

The stratification process of a fluid in an enclosed container is a long-standing classical problem (e.g. Elder 1965; Gill 1966; Batchelor 1954; Bergholz 1978; Patterson & Imberger 1980). A rudimentary experimental method is to place an initially homogeneous fluid in a rectangular cavity. If the top (bottom) horizontal wall is hot (cold), a stably stratified, vertically linear, temperature profile is established, by way of conduction, in the stagnant fluid. It is important in this situation that the vertical sidewalls are thermally insulated. The time needed for stratification is given by the diffusion timescale $O(H^2/\kappa)$. where H is the height of the cavity and κ the thermal diffusivity of fluid.

The classical work by Gill (1966) delineated the heat transfer characteristics in a vertical slot with different temperatures at the walls. Walin (1971), by dropping the assumption of perfectly conducting walls, derived a simplified equation for the density field in the interior. Expanding the approach of Walin (1971), a practically

† Author to whom correspondence should be addressed: e-mail jmhyun@cais.kaist.ac.kr

useful model of the stratification process was proposed by Rahm & Walin (1979*a*) and Rahm (1986). They allowed a small vertically upward mass flux, passing through the horizontal walls, as a means to facilitate stratification from an initially isothermal state. To better represent reality, the perfectly insulating condition at the vertical walls was also relaxed. Approximate equations which govern the transient stratifying process were suggested by Rahm (1986), and numerical solutions and physical implications were discussed by Hyun & Hyun (1986).

Another much-studied topic is heat-up, i.e. the transient adjustment process in response to temperature changes imposed at the vertical sidewall. The original model developers took note of the analogy between stratified and rotating fluids (e.g. Vernois 1970; Sakurai & Matsuda 1972; Jischke & Doty 1975; Hyun 1984, 1985, 1987). It was asserted that the overall stratifying process in the interior is controlled by convection and, therefore, is substantially accomplished over the heat-up timescale, which is an order-of-magnitude smaller than the diffusion timescale.

In the above two methodologies, the common theme is the initiation of convection, i.e. the bulk fluid motions, to expedite the stratifying process. In the former, the effect of forced convection by using a throughflow is the dominant factor. In the latter, buoyancy-driven convection, caused by the alteration in boundary-wall temperature, is the main ingredient. In the present account, the process of fluid stratification when the above two effects are comparable and simultaneously present is studied analytically.

In the present paper, a theoretical analysis is made of the behaviour of an initially stationary, stably stratified fluid in a square cavity. Fluid motion is initiated by introducing a vertical mass flux through the horizontal walls as well as a change in temperature at the vertical walls. The objective is to describe the flow details which are caused by the forced convection of the throughflow and by the buoyancy effect at the vertical walls. The analysis tackles the situation of practical interest in which the forced throughflow is comparable to the vertical flow induced in the buoyancy layer. Also, the vertical walls of the container are taken to be highly conducting. The problem posed is analogous to rotating flow, where the equivalent of the mass flux through the horizontal walls is a small difference in angular velocity of the container walls. The practical implications of the analogous rotating flow in geophysical fluid systems are obvious. The relevance of the flow studied here is in technological applications (see Gill 1966). Examples include thermal energy storage systems (Phillips & Dave 1982; Rahm 1986), efficient methods to produce a fluid of desired stratification in the laboratory (Walin 1971; Rahm & Walin 1979*a*; Hyun & Hyun 1986), and the concept of an ocean farm (Rahm & Walin 1979*b*) in which control of the interior fluid temperature is achieved by pumping cold fluid from below. To conduct an experimental simulation of the present problem, porous materials connected to constant-temperature baths can be used for the horizontal walls, and thin metallic plates of high thermal conductivity for the vertical walls.

In the majority of previous investigations (e.g. Walin 1971; Sakurai & Matsuda 1972; Jischke & Doty 1975; Hyun 1985, 1987), interest was confined to the interior core, far away from the boundary walls. Consequently, no explicit analysis of the boundary layer on the horizontal wall was given. Usually, the condition of global mass continuity was invoked to determine the flow characteristics in the interior. In this paper, for a more complete mathematical formulation, a thorough analysis of the horizontal boundary layer will be carried out. This will form an integral part of the overall analytical description of transient processes in the whole cavity.

The principal mathematical tool used here is matched asymptotic analysis. The

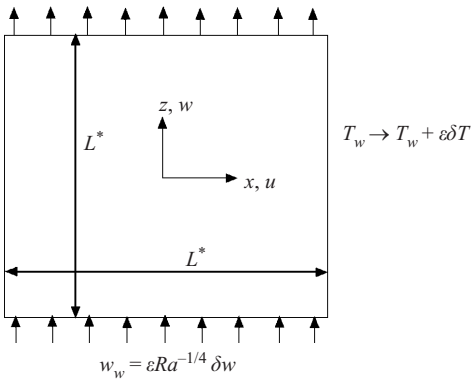

FIGURE 1. Problem definition and coordinate system.

effect of forced convection is measured by the intensity of throughflow (δw) imposed at the horizontal wall, and that of heat-up is gauged by the strength of thermal forcing (δT) at the vertical wall. Consideration will be given to the configurations when these two effects are opposing ($\delta w \delta T > 0$) or cooperative ($\delta w \delta T < 0$). Pertinent flow modes will be identified, and physical rationalizations will be given.

The mathematical model is given in § 2. Extensive use of the matched asymptotic method is made in § 3 to determine appropriate timescales and associated transient flow fields. Sections 4 and 5 contain, respectively, physical interpretations of the theoretical results for the opposing and cooperating cases. In § 6, to clarify the theoretical analysis, a comparison between numerical and theoretical solutions is given. A summary is given in § 7.

2. Mathematical formulation

A two-dimensional square enclosure with aspect ratio 1.0 is filled with an incompressible Boussinesq fluid (dynamic viscosity μ, thermal conductivity k, thermometric expansion coefficient β). The solid walls are assumed to be highly conducting. The flow layout and rectangular coordinates are sketched in figure 1. The choice of a square box represents the flow in a container of aspect ratio $O(1)$. A rectangular box may be studied with relative ease by one further scaling, and this feature will be dealt with in a forthcoming paper.

At the initial state, the fluid is stationary and is stably stratified in the vertical direction, i.e. the vertical fluid temperature distribution is

$$T_r^* = \frac{1}{2}\left\{(T_T^* + T_B^*) + (T_T^* - T_B^*)\frac{z^*}{L^*}\right\},$$

in which T_T^* and T_B^* are respectively the temperatures at the top and bottom horizontal walls, and L^* is the half-height.

Fluid motion is generated at the initial instant ($t^* = 0$) by simultaneous imposition of the two external disturbances, i.e. the temperature at the vertical walls is increased abruptly by δT^* and, at the same time, a uniform vertical throughflow δw^* is forced to pass through the top and bottom walls. The task is to depict the transient fluid response to the sudden imposition of these disturbances.

Non-dimensional quantities are defined (Jischke & Doty 1975) as

$$\nabla^* \equiv L^* \nabla,$$

$$p = \frac{p^* - p_r^*}{\varepsilon \rho_0^* g^* L^* \beta_0^* \Delta T^*},$$

$$T = \frac{T^* - T_r^*}{\varepsilon \Delta T^*},$$

$$(u, w) = (u^*, w^*) \frac{\sigma^{1/2}}{\varepsilon L^* N},$$

$$t = t^* N \sigma^{1/2},$$

in which $\Delta T^* \equiv T_T^* - T_B^*$, superscript * denotes dimensional quantities, subscript r refers to the initial state, subscript 0 indicates the reference value at the origin at the initial state. Also, $\varepsilon \ll 1$ represents the strength of external disturbances, the Prandtl number $\sigma = \mu_0^* C_{p0}^* / k_0^*$ and the Brunt–Väisälä frequency $N = (\beta_0^* \Delta T^* g^* / L^*)^{1/2}$.

The linearized, non-dimensional governing equations are

$$\frac{\partial u}{\partial x} + \frac{\partial w}{\partial z} = 0, \tag{1}$$

$$\frac{\partial u}{\partial t} = -\frac{\partial p}{\partial x} + Ra^{-1/2} \left(\frac{\partial^2 u}{\partial x^2} + \frac{\partial^2 u}{\partial z^2} \right), \tag{2}$$

$$\frac{\partial w}{\partial t} = -\frac{\partial p}{\partial z} + T + Ra^{-1/2} \left(\frac{\partial^2 w}{\partial x^2} + \frac{\partial^2 w}{\partial z^2} \right), \tag{3}$$

$$\sigma \frac{\partial T}{\partial t} + w = Ra^{-1/2} \left(\frac{\partial^2 T}{\partial x^2} + \frac{\partial^2 T}{\partial z^2} \right), \tag{4}$$

in which the Rayleigh number $Ra = \rho_0^{*2} g^* L^{*3} \beta_0^* \Delta T^* C_{\rho 0}^* / (k_0^* \mu_0^*)$.

For a definite problem formulation, at the initial instant $t = 0$, the thermal loading at the vertical walls is set at $\delta T \sim O(1)$, and the strength of throughflow is $Ra^{-1/4} \delta w$, $\delta w \sim O(1)$. These scalings imply that the effects of buoyancy-driven convection and of forced convection are comparable.

The associated initial and boundary conditions can be stated as

$$T = u = 0 \quad \text{at} \quad t = 0, \tag{5}$$

$$T[\equiv T_w] = \delta T, \quad u = w = 0 \quad \text{at} \quad x = \pm 1, \tag{6}$$

$$T = \delta T, \quad u = 0, \quad w[\equiv W_w] = Ra^{-1/4} \delta w \quad \text{at} \quad z = \pm 1. \tag{7}$$

3. Transient analysis of the heat-up timescale, $t \sim O(Ra^{1/4})$

For $Ra \gg 1$, the major features over $t \sim O(Ra^{1/4})$ can be characterized as: (i) quasi-steady buoyancy-driven boundary layers near the vertical walls, (ii) a transient inviscid interior, (iii) transient viscous boundary layers near the horizontal walls, and (iv) corner zones in which the horizontal and vertical boundary layers merge. These are sketched in figure 2 (see e.g. Walin 1971; Sakurai & Matsuda 1972; Jischke & Doty 1975). In view of symmetry of the problem, it suffices to consider only $0 \leqslant x \leqslant 1$.

The total solution Φ is written as $\Phi = \Phi_i + \Phi_{vb} + \Phi_{hb} + \Phi_c$, and analytical descriptions are sought by using the matched asymptotic method. Here, Φ stands for a flow

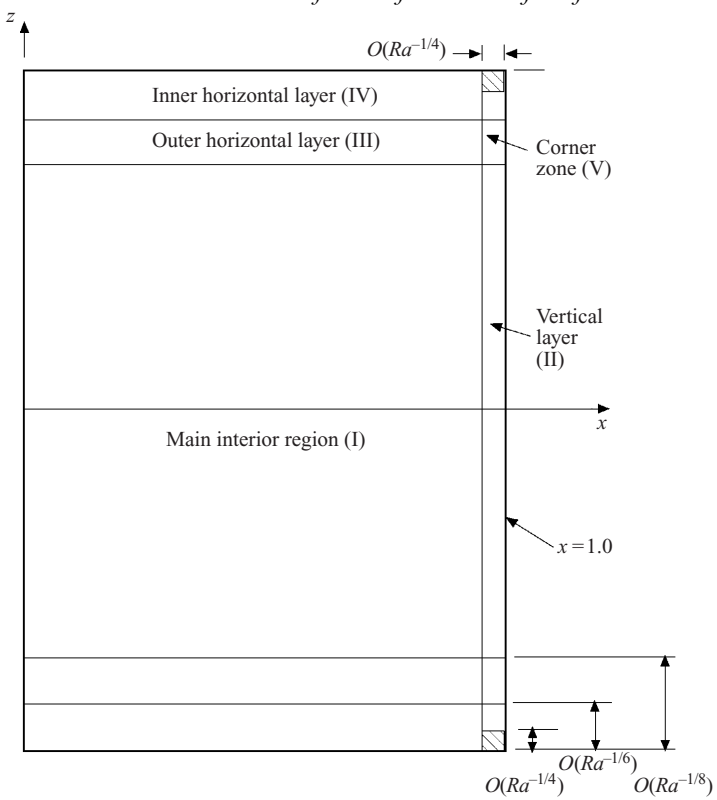

FIGURE 2. Characteristic flow regions.

variable, and subscripts i, vb, hb and c denote respectively the inviscid interior, vertical boundary layer, horizontal boundary layer and corner zone. As in previous studies (e.g. Sakurai & Matsuda 1972; Park & Hyun 1998), the principal lengthscales are $O(1)$ and $O(Ra^{-1/4})$ in the interior and in the vertical boundary layer. However, in the horizontal boundary layer, the lengthscales are double-structured, i.e. $O(Ra^{-1/6})$ and $O(Ra^{-1/8})$ (Veronis 1970; van Heijst 1982).

3.1. *Flow in the interior (region I)*

Time is rescaled by using the heat-up timescale, $\tau \equiv Ra^{-1/4}t$, and, guided by Jischke & Doty (1975), the lowest-order variables are

$$u = Ra^{-1/2}u_i, \quad w = Ra^{-1/4}w_i, \quad T = T_i, \quad p = p_i.$$

The governing equations are

$$\frac{\partial w_i}{\partial z} = 0. \tag{8a}$$

$$\frac{\partial p_i}{\partial x} = 0. \tag{8b}$$

$$\frac{\partial p_i}{\partial z} = T_i, \tag{8c}$$

$$\sigma\frac{\partial T_i}{\partial \tau} + w_i = 0. \tag{8d}$$

It is clear that w_i, T_i, and p_i are functions of τ only.

3.2. *Flow in the vertical boundary layer (region II)*

The vertical boundary layer is established over time $O(Ra^{-1/2})$, as elaborated in e.g. Sakurai & Matsuda (1972), Jischke & Doty (1975) and Park & Hyun (1998). Consequently, in the transient analysis of the heat-up timescale $O(Ra^{-1/4})$, the vertical boundary layer is taken to be quasi-steady.

The appropriate scalings in the vertical boundary layer are

$$u = Ra^{-1/2}(u_i + u_{vb}),$$
$$w = Ra^{-1/4}w_i + w_{vb},$$
$$T = T_i + T_{vb},$$
$$p = p_i + Ra^{-1/2}p_{vb},$$

and the horizontal coordinate is rescaled as $\eta = Ra^{1/4}(1 - x)$.

Substitution of the above variables into (1)–(4) yields

$$T_{vb} + \partial^2 w_{vb}/\partial\eta^2 = 0, \tag{9a}$$
$$w_{vb} - \partial^2 T_{vb}/\partial\eta^2 = 0. \tag{9b}$$

The boundary conditions at $\eta = 0$ are

$$w_{vb} = 0,$$

$$T_i + T_{vb} = \delta T,$$

and, as $\eta \to \infty$, $w_{vb}, T_{vb} \to 0$.

The solutions to (9*a*, *b*), subject to the above boundary conditions, are

$$T_{vb}(\tau, \eta) = (\delta T - T_i(\tau))\mathrm{e}^{-\eta/\sqrt{2}}\cos(\eta\sqrt{2}), \tag{10a}$$
$$w_{vb}(\tau, \eta) = (\delta T - T_i(\tau))\mathrm{e}^{-\eta/\sqrt{2}}\sin(\eta/\sqrt{2}). \tag{10b}$$

The remaining task is to determine $T_i(\tau)$. This can be easily accomplished by using the condition of global mass continuity, i.e.

$$\int_0^1 w_i \mathrm{d}x + \int_0^\infty w_{vb}\mathrm{d}\eta = \delta w. \tag{11}$$

Equations (8*d*), (10*b*) and (11) lead to

$$\sigma\frac{\partial T_i}{\partial\tau} + \frac{1}{\sqrt{2}}T_i = \frac{1}{\sqrt{2}}\delta T - \delta w. \tag{12a}$$

The solution to the above equation, subject to the initial condition $T_i(\tau = 0) = 0$, is

$$T_i(\tau) = (\delta T - \sqrt{2}\delta w)(1 - \mathrm{e}^{-\tau/(\sqrt{2}\sigma)}). \tag{12b}$$

It also follows from (8*d*) that

$$w_i(\tau) = \left(\delta w - \frac{\delta T}{\sqrt{2}}\right)\mathrm{e}^{-\tau/(\sqrt{2}\sigma)}. \tag{12c}$$

The results shown in (10) and (12) describe the transient flows in the interior and in the vertical boundary layers. However, the thrust of this paper is a more complete analysis of transient flow in the horizontal boundary layer. It will be asserted that this forms an essential part of the depiction of the heat-up process.

3.3. *Flow in the horizontal boundary layers* (*regions III and IV*)

The principal feature of the horizontal boundary layer is a double-layer structure, i.e. an inner layer of thickness $O(Ra^{-1/6})$ and an outer layer of thickness $O(Ra^{-1/8})$ (see Hunter 1967; van Heijst 1982). The inner layer satisfies the no-slip condition at the horizontal wall. The thicker outer layer matches the interior temperature to the horizontal wall temperature. Also, this layer transports fluid from the vertical layer to the interior, thereby causing heat-up in the interior. These notions were derived from the analogy between rotating and stratified fluids (see e.g. Veronis 1970).

The solution techniques follow the methodology proposed by van Heijst (1982). The variables in the horizontal boundary layer are expanded by using the expansion parameter $Ra^{-1/24}$. They are expressed as $\Phi_{hb} = \hat{\Phi} + \tilde{\Phi}$, in which the hat and the tilde refer to the outer ($Ra^{-1/8}$) and inner ($Ra^{-1/6}$) structure, respectively.

3.3.1. *Analysis for the* $Ra^{-1/8}$ *horizontal layer* (*region III*)

In line with the scalings suggested by van Heijst (1982),

$$u = Ra^{-1/2}u_i + Ra^{-1/8}\hat{u}_j,$$
$$w = Ra^{-1/4}w_i + Ra^{-1/4}\hat{w}_j,$$
$$T = T_i + \hat{T}_j,$$
$$p = p_i + Ra^{-1/8}\hat{p}_j,$$

and the boundary-layer coordinate $\xi_j = (1+(-1)^j z)Ra^{1/8}$ is introduced, where $j = 0, 1$ indicate, respectively, the lower and upper horizontal walls.

Rearranging (1)–(4) yields

$$(-1)^{j+1}\frac{\partial \hat{p}_j}{\partial \xi_j} + \hat{T}_j = 0, \tag{13a}$$

$$\sigma\frac{\partial \hat{T}_j}{\partial \tau} + \hat{w}_j = \frac{\partial^2 \hat{T}_j}{\partial \xi_j^2}, \tag{13b}$$

$$\frac{\partial \hat{p}_j}{\partial x} = 0, \tag{13c}$$

$$\frac{\partial \hat{u}_j}{\partial x} + (-1)^j\frac{\partial \hat{w}_j}{\partial \xi_j} = 0. \tag{13d}$$

The boundary conditions are

$$\hat{u}_j = \pm\frac{(-1)^{j+1}}{\sqrt{2}}\frac{\partial \hat{T}_j}{\partial \xi_j} \quad \text{at} \quad x = \pm 1, \tag{14a}$$

$$\hat{T}_j, \hat{w}_j \longrightarrow 0 \quad \text{as} \quad \xi_j \longrightarrow \infty, \tag{14b}$$

$$\left.\begin{aligned} T_i(\tau) + \hat{T}_j(\tau, x, \xi_j = 0) &= \delta T \\ w_i(\tau) + \hat{w}_j(\tau, x, \xi_j = 0) &= \delta w \end{aligned}\right\} \text{at} \quad \xi_j = 0. \tag{14c,d}$$

Condition (14*a*) is analogous to the Ekman compatibility condition in rotating flows, and the detailed derivation is given in the next section on the analysis of the corner zone.

From (13a), (13b) and (13c), it is obvious that $\hat{p}_j$, $\hat{T}_j$ and $\hat{w}_j$ are not functions of x, i.e.

$$\hat{p}_j = \hat{p}_j(\tau, \xi_j), \quad \hat{T}_j = \hat{T}_j(\tau, \xi_j) \quad \hat{w}_j = \hat{w}_j(\tau, \xi_j).$$

Equation (13d) is integrated to give

$$\hat{u}_j = (-1)^{j+1} \frac{\partial \hat{w}_j}{\partial \xi_j} x, \tag{15}$$

in which the integration constant is zero in view of the condition $\hat{u}_j(\tau, x = 0, \xi_j) = 0$. From (14$a$) and (15),

$$\hat{T}_j = \sqrt{2}\hat{w}_j, \tag{16}$$

and, from (8d), (14c) and (14d), the equation for $T_i(\tau)$ is obtained:

$$\sigma \frac{\partial T_i}{\partial \tau} + \frac{1}{\sqrt{2}} T_i = \frac{1}{\sqrt{2}} \delta T - \delta w. \tag{17a}$$

The solution to (17a) is readily found as

$$T_i(\tau) = (\delta T - \sqrt{2}\delta w)(1 - \mathrm{e}^{-\tau/(\sqrt{2}\sigma)}). \tag{17b}$$

As anticipated, the equation and solution for $T_i(\tau)$, expressed in (17a) and (17b), are identical to those for $T_i(\tau)$, shown in (12a) and (12b), which were obtained on the basis of global mass continuity condition.

The equation for the temperature in the horizontal boundary layer is derived by using (13b) and (16):

$$\sigma \frac{\partial \hat{T}_j}{\partial \tau} + \frac{\hat{T}_j}{\sqrt{2}} = \frac{\partial^2 \hat{T}_j}{\partial \xi_j^2}. \tag{18}$$

The solution to (18), subject to the initial condition $\hat{T}_j(0, \xi_j) = 0$ and the boundary conditions (14b) and (14c), is

$$\begin{aligned} \hat{T}_j(\tau, \xi_j) = \sqrt{2}\hat{w}_j(\tau, \xi_j) = (\delta T - \sqrt{2}\delta w)\mathrm{erfc}\left(\frac{\xi_j}{2}\sqrt{\frac{\sigma}{\tau}}\right) \exp\left(-\frac{\tau}{\sqrt{2\sigma}}\right) \\ + \sqrt{2}\delta w \left\{ \exp(-\xi_j/x) - \frac{1}{2}\exp(-\xi_j/x)\mathrm{erfc}\left(\sqrt{\tau/(x^2\sigma)} - \frac{\xi_j}{2\sqrt{\tau/\sigma}}\right) \right. \\ \left. + \frac{1}{2}\exp(\xi_j/x)\mathrm{erfc}\left(\sqrt{\tau/(x^2\sigma)} + \frac{\xi_j}{2\sqrt{\tau/\sigma}}\right) \right\}, \end{aligned} \tag{19a}$$

in which $x = \sqrt[4]{2}$.

Also, $\hat{u}_j$ is determined from (15):

$$\begin{aligned} \hat{u}_j(\tau, x, \xi_j) = \frac{(-1)^j}{2}\sqrt{\frac{\sigma}{2\pi\tau}}(\delta T - \sqrt{2}\delta w)x \exp\left(-\frac{\sigma\xi_j^2}{4\tau} - \frac{\tau}{\sqrt{2\sigma}}\right) \\ + \frac{(-1)^j}{x}\delta w x \left\{ \exp(-\xi_j/x) - \frac{1}{2}\exp(-\xi_j/x)\mathrm{erfc}\left(\sqrt{\tau/(x^2\sigma)} - \frac{\xi_j}{2\sqrt{\tau/\sigma}}\right) \right. \\ \left. - \frac{1}{2}\exp(\xi_j/x)\mathrm{erfc}\left(\sqrt{\tau/(x^2\sigma)} + \frac{\xi_j}{2\sqrt{\tau/\sigma}}\right) \right\}. \end{aligned} \tag{19b}$$

The above procedure provides a complete analytical description of the $Ra^{-1/8}$

boundary layer. It is noted that the horizontal velocity at the wall does not satisfy the no-slip condition. This will be taken care of by matching the above solution to the solution for the $Ra^{-1/6}$ boundary layer.

3.3.2. *Analysis of the $Ra^{-1/6}$ layer (region IV)*

Again, in accordance with van Heijst (1982), the appropriate scalings are:

$$u = Ra^{-1/2}u_i + Ra^{-1/8}\hat{u}_j + Ra^{-1/8}\tilde{u}_j,$$
$$w = Ra^{-1/4}w_i + Ra^{-1/4}\hat{w}_j + Ra^{-7/24}\tilde{w}_j,$$
$$T = T_i + \hat{T}_j + Ra^{-1/8}\tilde{T}_j,$$
$$p = p_i + Ra^{-1/8}\hat{p}_j + Ra^{-7/24}\tilde{p}_j,$$

and the boundary-layer coordinate $\zeta_j = (1 + (-1)^j z)Ra^{1/6}$ is introduced, in which $j = 0$ and $j = 1$ denote respectively the lower and upper horizontal walls.

Substitution of the above into (1)–(4) yields

$$-(-1)^j \frac{\partial \tilde{p}_j}{\partial \zeta_j} + \tilde{T}_j = 0, \tag{20a}$$

$$\tilde{w}_j = \frac{\partial^2 \tilde{T}_j}{\partial \zeta_j^2}, \tag{20b}$$

$$-\frac{\partial \tilde{p}_j}{\partial x} + \frac{\partial^2 \tilde{u}_j}{\partial \zeta_j^2} = 0, \tag{20c}$$

$$\frac{\partial \tilde{u}_j}{\partial x} + (-1)^j \frac{\partial \tilde{w}_j}{\partial \zeta_j} = 0. \tag{20d}$$

The associated boundary conditions are

$$\tilde{u}_j, \tilde{w}_j, \tilde{T}_j \to 0 \quad \text{as} \quad \zeta_j \to \infty, \tag{21a}$$

$$\tilde{u}_j(\tau, x, \zeta_j \to 0) = -\hat{u}_j(\tau, x, \xi_j \to 0), \quad \tilde{w}_j = \tilde{T}_j = 0 \quad \text{as} \quad \zeta_j = 0, \tag{21b}$$

$$\tilde{u}_j = 0 \quad \text{at} \quad x = \pm 1. \tag{21c}$$

Equations (20*a*), (20*b*) and (20*c*) lead to

$$\frac{\partial \tilde{T}_j}{\partial x} = (-1)^j \frac{\partial^3 \tilde{u}_j}{\partial \zeta_j^3}, \tag{22a}$$

$$\frac{\partial \tilde{w}_j}{\partial x} = (-1)^j \frac{\partial^5 \tilde{u}_j}{\partial \zeta_j^5}. \tag{22b}$$

Also, together with (20*d*), one finds

$$\frac{\partial^2 \tilde{u}_j}{\partial x^2} + \frac{\partial^6 \tilde{u}_j}{\partial \zeta_j^6} = 0. \tag{23}$$

The solution to (23) is taken to be of the form

$$\tilde{u}_j(\tau, x, \zeta_j) = \sum_{n=1}^{\infty} U_n(\tau, \zeta_j) \sin(n\pi x), \tag{24}$$

and the boundary conditions are

$$U_n = F_n = (\tau), \quad \frac{\partial^3 U_n}{\partial \zeta_j^3} = 0, \quad \frac{\partial^5 U_n}{\partial \zeta_j^5} = 0 \quad \text{as} \quad \zeta_j \to 0.$$

in which

$$F_n(\tau) = (-1)^{n+j}\frac{4}{n\pi}\left\{(\delta T - \sqrt{2}\delta w)\sqrt{\frac{\sigma}{\pi\tau}}\exp\left(-\frac{\tau}{\sqrt{2\sigma}}\right) + x\,\delta w\,\mathrm{erf}\left(\frac{1}{x}\sqrt{\frac{\tau}{\sigma}}\right)\right\}.$$

Placing (24) into (23) results in

$$U_n(\tau, \zeta_j) = F_n(\tau)\left\{\frac{\exp(-\omega_n\zeta_j)}{2} + \exp(-\omega_n\zeta_j/2)\cos\left(\frac{\pi}{3} + \sqrt{3}\omega_n\zeta_j/2\right)\right\}$$

where $\omega_n = (n\pi)^{1/3}$.

3.4. *Analysis of the corner zone (region V)*

The vertical and horizontal boundary layers merge in the corner zones (of size $Ra^{-1/4} \times Ra^{-1/8}$), shown by region V in figure 2. For this zone, stretched coordinates are introduced, i.e. $\eta = Ra^{1/4}(1 - x)$ and $\xi_j = Ra^{1/8}(1 + (-1)^j z)$ $(j = 0, 1)$. The appropriate scalings for the corner zone are

$$\begin{aligned} u &= Ra^{-1/2}u_i + Ra^{-1/2}u_{vb} + Ra^{-1/8}\hat{u}_j + Ra^{-1/8}\hat{\hat{u}}_j, \\ w &= Ra^{-1/4}w_i + w_{vb} + Ra^{-1/4}\hat{w}_j + \hat{\hat{w}}_j, \\ T &= T_i + T_{vb} + \hat{T}_j + \hat{\hat{T}}_j, \\ p &= p_i + Ra^{-1/2}p_{vb} + Ra^{-1/8}\hat{p}_j + Ra^{-1/2}\hat{\hat{p}}_j. \end{aligned}$$

Substituting the above into (1)–(4) for the corner zone results in

$$\frac{\partial \hat{\hat{w}}_j}{\partial \xi_j} - (-1)^j\frac{\partial \hat{\hat{u}}_j}{\partial \eta} = 0, \tag{25a}$$

$$\hat{\hat{T}}_j + \frac{\partial^2 \hat{\hat{w}}_j}{\partial \eta^2} = 0, \tag{25b}$$

$$\hat{\hat{w}}_j - \frac{\partial^2 \hat{\hat{T}}_j}{\partial \eta^2} = 0, \tag{25c}$$

with the boundary conditions

$$\hat{u}_j(\tau, x = 1, \xi_j) + \hat{\hat{u}}_j(\tau, \eta \to 0, \xi_j) = 0, \tag{26a}$$

$$\hat{\hat{w}}_j(\tau, \eta \to 0, \xi_j) = 0, \tag{26b}$$

$$\hat{T}_j(\tau, x = 1, \xi_j) + \hat{\hat{T}}_j(\tau, \eta \to 0, \xi_j) = 0 \quad (j = 0, 1), \tag{26c}$$

$$\hat{\hat{u}}_j, \hat{\hat{w}}_j, \hat{\hat{T}}_j \to 0 \quad \text{as} \quad \eta \to \infty \quad \text{or} \quad \xi_j \to \infty, \tag{26d}$$

The solutions to (25*b*), (25*c*) are

$$\hat{\hat{T}}_j = -\hat{T}_j e^{-\eta/\sqrt{2}}\cos(\eta/\sqrt{2}), \tag{27a}$$

$$\hat{\hat{w}}_j = -\hat{T}_j e^{-\eta/\sqrt{2}}\sin(\eta/\sqrt{2}). \tag{27b}$$

Also, integrating (25*a*) gives

$$\hat{\hat{u}}_j = \frac{(-1)^j}{\sqrt{2}} \frac{\partial \hat{T}_j}{\partial \xi_j} \mathrm{e}^{-\eta/\sqrt{2}} [\sin(\eta/\sqrt{2}) + \cos(\eta/\sqrt{2})]. \tag{27c}$$

Combining (26*a*) and (27*c*), the compatibility condition, which links the ($Ra^{-1/4} \times Ra^{-1/8}$) corner zone and the horizontal boundary layers, is obtained:

$$\hat{u}_j(\tau, r = 1, \xi_j) = \frac{(-1)^{j+1}}{\sqrt{2}} \frac{\partial \hat{T}_j}{\partial \xi_j}. \tag{28}$$

The above relationship is analogous to the well-known Ekman compatibility condition in rotating fluids (see e.g. Greenspan 1968).

In summary, the streamfunction Ψ can be computed as

$$\begin{aligned} \Psi(\tau, x, z) &= \int_0^x w \mathrm{d}x \\ &= \int_0^x \left\{ Ra^{-1/4} w_i + w_{vb} + \sum_{j=0}^{1} (Ra^{-1/4} \hat{w}_j + Ra^{-7/24} \tilde{w}_j + \hat{\hat{w}}_j) \right\} \mathrm{d}x. \end{aligned} \tag{29a}$$

The fourth term in the above integral, $\int_0^x Ra^{-7/24} \tilde{w}_j \mathrm{d}x$, can, in principle, be calculated from (22*b*) and (24). However, this operation is tedious and time-consuming. Under the assumption $Ra \gg 1$, this term is smaller than the other terms, which are $O(Ra^{-1/4})$, and therefore can be neglected in (29*a*). It then follows that

$$\begin{aligned} \Psi(\tau, x, z) \approx\ & Ra^{-1/4} \left(w_i(\tau) + \sum_{j=0}^{1} \hat{w}_j(\tau, \xi_j) \right) x \\ & + Ra^{-1/4} \left(\delta T - T_i(\tau) - \sum_{j=0}^{1} \hat{T}_j(\tau, \xi_j) \right) \mathrm{e}^{-\eta/\sqrt{2}} \sin(\eta/\sqrt{2} + \pi/4). \end{aligned} \tag{29b}$$

It is noted that T_i and w_i are given in (12*b*) and (12*c*), and $\hat{T}_j$ and $\hat{w}_j$ are given in (19*a*), and, $\eta = Ra^{1/4}(1-x)$ and $\xi_j = Ra^{1/8}(1+(-1)^j z)$. In (29*a*), the third and fourth terms refer, respectively, to the flows in the $Ra^{-1/8}$-layer and $Ra^{-1/6}$-layer. The fact that the third term is smaller than the fourth term implies that, in the limit $Ra \gg 1$, most of the mass transport is accomplished through the $Ra^{-1/8}$-layer. The dynamical role of the $Ra^{-1/8}$-layer is two-fold: (i) it matches the temperature in the interior to the temperature at the horizontal wall, and (ii) it carries the mass transport from the horizontal wall to the interior as well as to the vertical boundary layer. The overall character of the $Ra^{-1/8}$-layer is analogous to the outer Stewartson layer of thickness $O(E^{1/4})$, where E is the Ekman number, which appears in rotating flows in a cylinder with mass fluxes imposed at the cylindrical sidewall (e.g. Barcilon 1968).

As remarked previously, the no-slip condition at the horizontal wall is met by the $Ra^{-1/6}$ horizontal layer. It may now be stated that, in the present problem, the outer layer is more important than the inner layer in setting up the interior motion.

4. The global adjustment process: opposing configuration ($\delta w \delta T > 0$)

With $\delta w > 0 (\delta w < 0)$, the effect of throughflow is to cool down (heat up) the interior; and, $\delta T > 0 (\delta T < 0)$ causes the interior to heat up (cool down).

Therefore, the condition $\delta w \delta T > 0$, indicates opposite contributions to the interior. For simplicity, we take $\delta w > 0$ and $\delta T > 0$.

4.1. *Relative magnitudes of* δw *and* δT

As revealed in the foregoing analysis, $\delta w/\delta T$ represents the ratio of the effect of forced convection of throughflow at the horizontal wall to the effect of buoyant convection of thermal loading at the vertical wall. Also, the physical meaning of $\delta w/\delta T$ can be seen in the grouping of nondimensional parameters:

$$\frac{\delta w}{\delta T} = \left(\frac{W_w^* \sigma^{1/2} Ra^{1/4}}{L^* N}\right) \Big/ \left(\frac{T_w^* - T_r^*}{T_T^* - T_B^*}\right) = Gr_H^{-1} Re_H^{-1}$$

where

$$Gr_H = \frac{k_0^*}{\mu_0^* C_{p0}^*} \frac{\rho_0^{*2} g^* L^{*3} \beta_0^* (T_w^* - T_r^*) C_{p0}^*}{\mu_0^* k_0^*},$$

$$Re_H = \frac{\rho_0^* W_w^* R^*}{\mu_0^*},$$

R^* denoting the thickness of the vertical boundary layer, i.e. $R^* \equiv L^*\, Ra^{-1/4}$. Obviously, Gr_H is the Grashof number based on the horizontal temperature contrast; and Re_H the Reynolds number in the vertical boundary layer. In summary, $\delta w/\delta T$ is the mixed-convection parameter, representing the strength of forced convection relative to that of buoyancy convection.

The preceding analysis in § 3 established a criterion for the magnitude of $\delta w/\delta T$, i.e. the general flow character can be classified according to $\delta w/\delta T \gtrless 1/\sqrt{2}$. The dominant features of the transient process can be characterized by the forced-convection-dominant mode ($\delta w/\delta T > 1/\sqrt{2}$), the nearly static mode ($\delta w/\delta T \approx 1/\sqrt{2}$), and the buoyancy-convection-dominant mode ($0 < \delta w/\delta T < 1/\sqrt{2}$).

4.2. *Forced-convection-dominant mode* ($\delta w/\delta T > 1/\sqrt{2}$)

Plots of the transient flow pattern for $\delta w/\delta T > 1/\sqrt{2}$ are calculated by using equation (29*b*) and illustrated in figure 3. It is discernible that the vertical boundary layer is formed in time $t \sim O(1)$, which is much shorter than the heat-up timescale. This again justifies the treatment of vertical boundary layer as being quasi-steady. The fluid transport carried upward in the vertical boundary layer, Q_{VB}, can be computed using (10*b*) and (12*b*):

$$Q_{VB} = 2Ra^{-1/4} \int_0^\infty w_{vb}(\tau, \eta) \mathrm{d}\eta = 2Ra^{-1/4} \delta w + (\sqrt{2}\delta T - 2\delta w) Ra^{-1/4} \exp(-\tau/(\sqrt{2}\sigma)). \quad (30a)$$

As seen in the definition of the problem, the first term on the right-hand side of (30*a*) indicates the fluid intake. Q_{HW} through the bottom horizontal wall, i.e.

$$Q_{HW} = 2Ra^{-1/4} \delta w. \quad (30b)$$

If $\delta w/\delta T > 1/\sqrt{2}$, the second term on the right-hand side of (30*a*) is negative, which implies that, in the transient stage, $Q_{VB} < Q_{HW}$. This further demonstrates that the vertical boundary layer cannot transport upward all the fluid that has entered through the bottom horizontal wall. Therefore, part of the fluid influx is

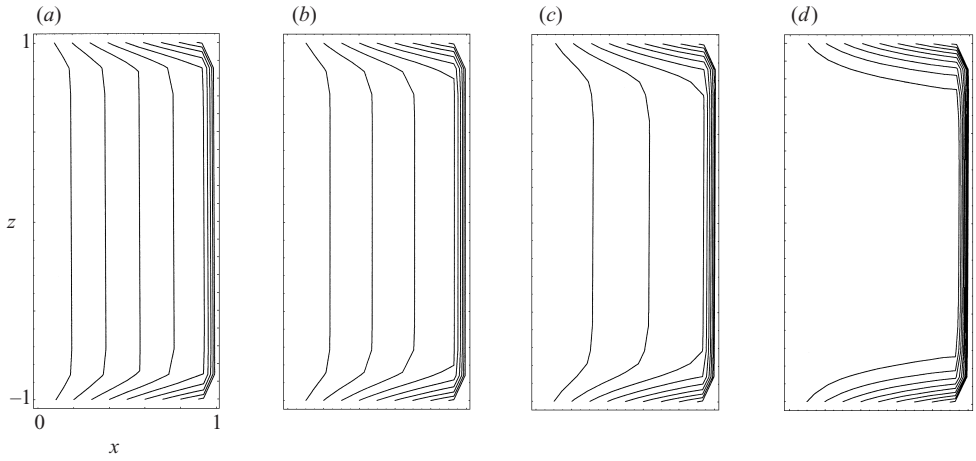

FIGURE 3. Plots of the stream function for the forced-convection-dominant mode ($\delta w = 2.0$, $\delta T = 1.0$); $\sigma = 1.0$ and $Ra = 10^8$. Times, τ, are: (*a*) 0.3; (*b*) 0.6; (*c*) 1.0; (*d*) ∞. The contour increment is $0.1 \times Ra^{-1/4}\delta w$.

transported upward directly through the inviscid interior to reach the horizontal boundary layer at the top wall (see figures 3*b* and *c*). In the inviscid interior (region I), the vertical motions bring up the cold fluid from below, which causes cool-down. At the same time, the temperature difference between the interior and the vertical wall increases, which, in turn, invigorates the buoyancy-driven motion in the vertical boundary layer. This strengthened vertical layer carries upward a larger amount of fluid; therefore, the vertical transports in the interior weaken (see figure 3*c*). Following these processes, the bulk of the inviscid interior evolves to a new state of equilibrium, i.e. as $\tau \to \infty$, $T_i \to \delta T - \sqrt{2}\delta w$, which is portrayed in equation (12*b*). The global transient adjustment for the case $\delta w/\delta T > 1/\sqrt{2}$ is depicted in figure 3. As observed earlier, the principal transient characteristics in the inviscid interior are controlled more by forced convection through the horizontal wall than by bouyancy-driven convection near the vertical wall. These aspects are in accord with the general findings in §4.1. In the steady state, the entire fluid transport is concentrated in horizontal and vertical boundary layers, and the inviscid interior is stagnant and stably stratified (see figure 3*c*). These patterns are in line with previous assertions (e.g. Rahm & Walin 1979; Hyun & Hyun 1986).

The vertical profiles of the evolving temperature T and vertical velocity w near the horizontal wall are shown in figure 4. Immediately after the simultaneous switch-on of thermal loading ($\delta T = 1.0$) and of throughflow ($\delta w = 2.0$) at the horizontal wall, both T and w decrease rapidly, due to diffusion from the wall and forced convection of the upward throughflow, in the close vicinity of the horizontal wall. As the inviscid interior region is approached, diffusion from the wall diminishes, and T and w settle to uniform values, nearly independent of height. As time elapses, the thickness of the boundary layer increases; also, as the cool-down due to vertically upward transport proceeds. T decreases further in the interior. The magnitude of w is largest at the horizontal wall because part of the throughflow moves to the vertical boundary layer along the horizontal layer, and w decreases and settles to a uniform value as the interior is approached.

In summary, in the forced-convection-dominant mode, the inviscid interior cools down due to the vertically upward fluid motions during the transient phase. With

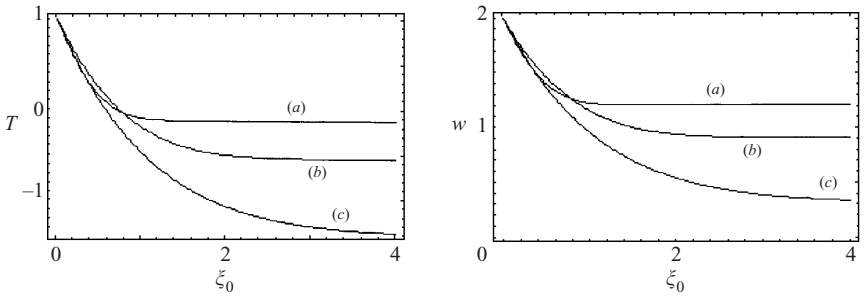

FIGURE 4. Evolution of temperature, T, and vertical velocity, w, fields for the forced-convection-dominant mode ($\delta w = 2.0$, $\delta T = 1.0$). Times, τ, are: (a) 0.1; (b) 0.5; (c) 2.0; $\sigma = 1.0$ and $Ra = 10^8$. $\xi_0 = (1+z)Ra^{1/8}$.

passage of time, w in the interior diminishes, indicating the end of the transient phase. As ascertained earlier, with the cooling down of the interior, the vertical boundary layer is intensified. This allows the fluid transported vertically upward to be carried into the vertical boundary layer.

4.3. *Buoyant-convection-dominant mode* ($0 < \delta w/\delta T < 1/\sqrt{2}$)

When $0 < \delta w/\delta T < 1/\sqrt{2}$, over the transient phase, the second term on the right-hand side of (30a) becomes positive, which means that $Q_{HW} < Q_{VB}$. This implies that the fluid pumped upward by the vertical boundary layer, Q_{VB}, is larger than the fluid intake by throughflow at the bottom horizontal wall, Q_{HW}. Put differently, the entire volume of throughflow forms part of the vertical boundary layer transport. Near the top horizontal wall, since $Q_{HW} < Q_{VB}$, all of the transport by the vertical boundary layer cannot be accommodated by the discharge through the top horizontal wall. Naturally, part of Q_{VB} has to return to the inviscid interior, which gives rise to vertically downward motions in the interior. These downward motions bring hot fluid from above, and, at a given location in the interior, heat-up occurs, and the fluid temperature rises as time elapses. With the increasing interior temperature, the difference in temperature between the interior and vertical walls decreases, which weakens the motion in the vertical boundary layer. The overall pattern of the time-dependent process is depicted by the above scenario: as time passes, the state in which $Q_{HW} \approx Q_{VB}$ is reached, and the interior approaches a new equilibrium state, i.e. a stagnant interior with $T_i(\tau \to \infty) \approx \delta T - \sqrt{2}\delta w$.

This characteristic transient behaviour is described by equations (12b) and (30), and is portrayed in figure 5 for the case $0 < \delta w/\delta T < 1/\sqrt{2}$. In short, the interior motions are influenced more by buoyant effects in the vertical boundary layer than by forced-convection effects of throughflow at the horizontal wall.

The evolutions of w and T near the bottom horizontal wall are exhibited in figure 6. Immediately after the switch-on of δw and δT, both w and T decrease rapidly away from the wall due to diffusion from the wall. After ξ passes the edge of the boundary layer, w and T approach uniform values in the inviscid interior. It is noted, however, that, in contrast to the forced-convection-dominant mode, the value of T in the interior increases with time. This reflects the aforementioned heat-up process in the interior, which emanates from buoyancy effects in the vertical boundary layer. The vertical motions in the interior are initially downward (w negative), and, as time elapses, fluid in the interior becomes stagnant (w approaches zero). Again, as time

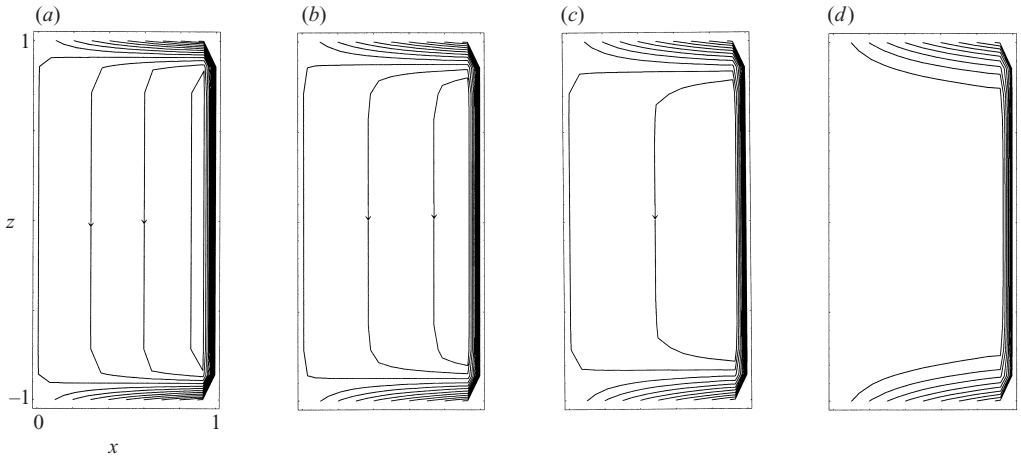

FIGURE 5. Plots of the stream function for the buoyant-convection-dominant mode ($\delta w = 1/2$, $\delta T = 1.0$); $\sigma = 1.0$ and $Ra = 10^8$. Times, τ, are: (*a*) 0.3; (*b*) 0.6; (*c*)1.0; (*d*) ∞. The contour increment is $0.1 \times Ra^{-1/4}\delta w$.

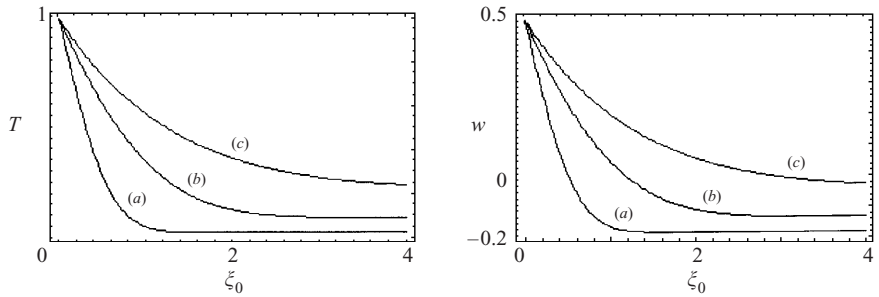

FIGURE 6. Evolution of temperature, T, and vertical velocity, w, fields for the buoyant-convection-dominant mode ($\delta w = 1/2$, $\delta T = 1.0$). Times, τ, are: (*a*) 0.1; (*b*) 0.5; (*c*) 2.0. $\sigma = 1.0$ and $Ra = 10^8$, $\xi_0 = (1 + z)Ra^{1/8}$.

progresses, the mass transport in the vertical boundary layer is decreased, since the temperature difference between the interior and vertical walls becomes small.

4.4. *Static mode* ($\delta w/\delta T \approx 1/\sqrt{2}$)

As is apparent in equation (12*b*) and (12*c*), if $\delta w/\delta T \approx 1/\sqrt{2}$, the interior fluid maintains the initial conditions ($T_i(\tau) = 0$ and $w_i(\tau) = 0$) over the heat-up phase $t \sim O(Ra^{1/4})$. In this case, the vertical boundary layer is established at $t \sim O(1)$, which is much shorter than the heat-up time $t \sim O(Ra^{1/4})$; and the vertical layer completely accommodates the transport of the throughflow. Therefore, the fluid intake by throughflow moves in the horizontal boundary layer toward the vertical wall, and is carried upward in the vertical boundary layer. Near the top horizontal wall, this vertical-layer transport then moves along the horizontal boundary layer, and, finally is discharged to the outside vertically through the top horizontal wall. In short, the global flow pattern in the static mode is similar to the steady-state flow of the two previous modes, which were shown in figures 3(*d*) and 5(*d*). In the static mode, the pertinent timescale is $t \sim O(1)$, which corresponds to dimensional time $t^* \sim O(N^{-1}\sigma^{-1/2})$, in all the region except the horizontal boundary layer. In this layer,

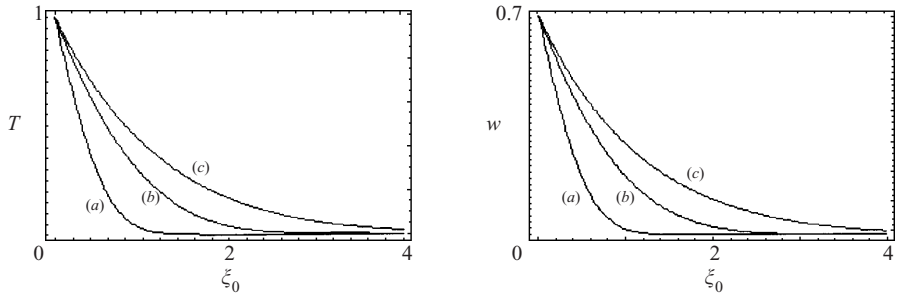

FIGURE 7. Evolution of temperature, T, and vertical velocity, w, fields for the static mode ($\delta w = 1/\sqrt{2}$, $\delta T = 1.0$). Times, τ, are: (a) 0.1; (b) 0.5; (c) 2.0. $\sigma = 1.0$ and $Ra = 10^8$. $\xi_0 = (1+z)Ra^{1/8}$.

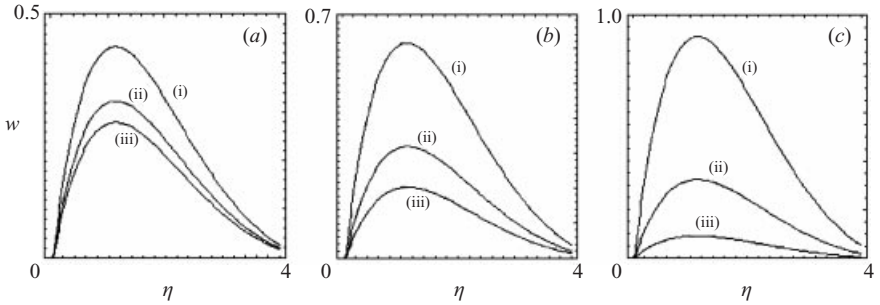

FIGURE 8. Profiles of vertical velocity, w, in the vertical boundary layer. Times, τ, are: (a) 0.3; (b) 1.0; (c) ∞. The values (δw, δT) are: (i) $\delta w = 2.0$, $\delta T = 1.0$ (forced-convection-dominant mode); (ii) $\delta w = 1/\sqrt{2}$, $\delta T = 1.0$ (static mode); (iii) $\delta w = 0.2$, $\delta T = 1.0$ (buoyant-convection-dominant mode). $\sigma = 1.0$ and $Ra = 10^8$, $\eta = (1-x)Ra^{1/4}$.

the steady state is reached at $t \sim O(Ra^{1/4})$. In other words, in the heat-up phase, the time-dependent features are discernible only in the horizontal boundary layer, and flows in the other regions are essentially steady.

Evolutionary vertical profiles of T and w in the vicinity of the bottom horizontal wall are illustrated in figure 7. The initial development of the horizontal boundary layer, which is due to diffusion from the wall, is similar to that of the two previous modes. In the interior, however, both w and T approach zero at all times, which is unique to the static mode.

The qualitative differences in the transient flow character in the vertical boundary layer of the above three modes are shown in figure 8. As asserted earlier, the inviscid interior region cools down, which is influenced by throughflow, in the forced-convection mode. In contrast, in the buoyant-convection mode, the interior region heats up, which is dominated by buoyancy effects in the vertical boundary layer. In the static mode, the interior remains in the initial-state equilibrium. Consequently, with the passage of time, the temperature difference between the interior and vertical wall (i) increases in the forced-convection mode, (ii) decreases in the buoyant-convection mode, and (iii) remains unchanged in the static mode. Accordingly, the strength of the vertical boundary layer, as represented by w in figure 8, (i) increases, (ii) decreases, and (iii) remains unchanged, in the respective modes.

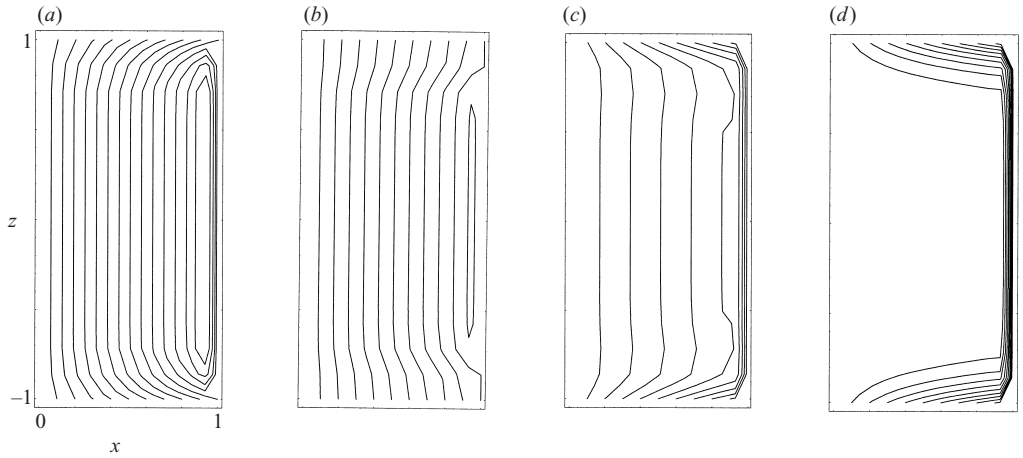

FIGURE 9. Plots of the stream function for the buoyant-convection-dominant mode ($\delta w = 1.0$, $\delta T = -2.0$). $\sigma = 1.0$ and $Ra = 10^8$. Times, τ, are: (*a*) 0.6; (*b*) 1.0; (*c*) 2.0; (*d*) ∞. The contour increment is $0.1 \times Ra^{-1/4}\delta w$.

5. The global adjustment process: cooperating configuration ($\delta w \delta T < 0$)

The cooperating configuration refers to the situation when both the forced-convection effect and the buoyancy effect act to heat up (or cool down) the interior fluid. For definiteness, an example of cool-down ($\delta w > 0$, $\delta T < 0$) will be dealt with ($\delta w = 1.0$, $\delta T = -2.0$).

As displayed in figure 9(*a*), at small times, the cooling ($\delta T < 0$) of the vertical wall induces downward flows in the vertical boundary layer. This induces clockwise-circulating motions in the entire right half-cavity, which causes the fluid transport of throughflow to move directly upward in the interior. With the passage of time, due to the intrusion of cold throughflow, the interior cools down, which, in turn, lowers the temperature difference between the interior and the vertical wall. Consequently, motions in the vertical boundary layer weaken, and the clockwise-circulating flow tends to be localized close to the vertical wall (see figure 9*b*). As cool-down of the interior progresses, the temperature of the interior becomes lower than that of the vertical wall. This reverses the direction of buoyancy; therefore, in the vertical boundary layer, a rising motion takes place (see figure 9*c*). After this stage has been reached, the transient behaviour is akin to that of the forced-convection mode of the opposing configuration (see figure 9*c*, *d*). At the final stage (figure 9*d*), as expected, the majority of fluid is carried via the boundary layers, and the interior is occupied by stratified stagnant fluid.

Figure 10 portrays the evolution of vertical profiles of T and w near the bottom horizontal wall. The cool-down of the interior is discernible. It is observed that, at very small times (e.g. see the curve for $\tau = 0.1$ of figure 10*b*), the magnitude of the vertical velocity $w_i[\equiv w(\tau = 0.1, \xi \to \infty)]$ in the interior is larger than the vertical intake throughflow velocity (δw) at the horizontal wall. This is because of the formation of clockwise-circulating flows (see figure 9*a*). These flows push the original vertically oriented throughflow toward the cavity centreline ($x = 0$), which reduces the effective flow passage area. It is recalled that, in the forced-convection-dominant mode of the opposing configuration, part of the interior vertical fluid transport is added to the flow in the vertical boundary layer, which results in $w_i < \delta w$.

One notable feature of the cooperating configuration is the presence of clockwise-

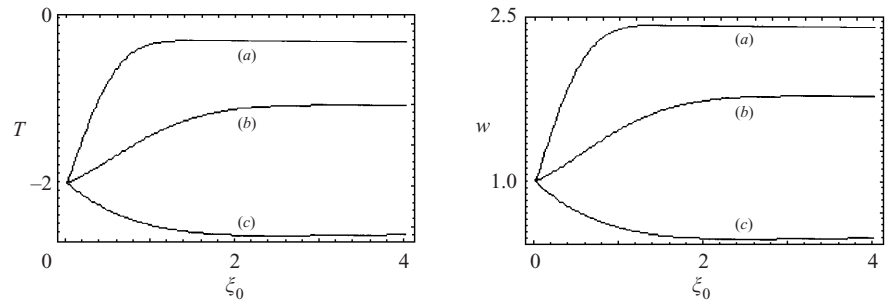

FIGURE 10. Evolution of temperature, T, and vertical velocity, w, fields for the static mode ($\delta w = 1.0$, $\delta T = -2.0$). Times, τ, are: (*a*) 0.1; (*b*) 0.5; (*c*) 2.0. $\sigma = 1.0$ and $Ra = 10^8$, $\xi_0 = (1+z)Ra^{1/8}$.

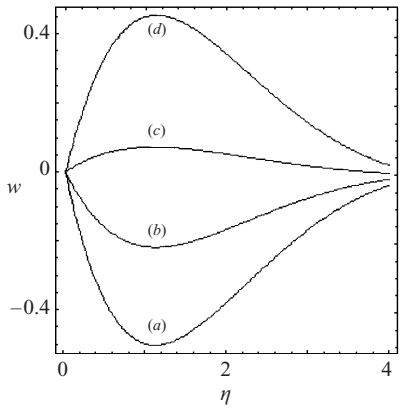

FIGURE 11. Profiles of vertical velocity, w, fields in the vertical boundary layer ($\delta w = 1.0$, $\delta T = -2.0$). Times, τ, are: (*a*) 0.2; (*b*) 0.7; (*c*) 1.5; (*d*) ∞. $\sigma = 1.0$ and $Ra = 10^8$. $\eta = (1-x)Ra^{1/4}$.

circulating flow at small times. As emphasized earlier, this flow pattern disappears after some time ($\tau = \tau_c$), and the time-dependent flow characteristics after this time, i.e. $\tau > \tau_c$, are similar to those of the forced-convection mode of the opposing configuration. In an effort to gauge τ_c, it is noted that in (10*b*) the maximum velocity $(w_{vb})_{max}$ in the vertical boundary layer occurs at $\eta = \pi/4$:

$$[w_{vb}(\tau, \eta = \sqrt{2}\pi/4)]_{max} = (\delta T - T_i(\tau))\frac{e^{-\pi/4}}{\sqrt{2}}$$
$$= [\sqrt{2}\delta w + (\delta T - \sqrt{2}\delta w)e^{-\tau/(\sqrt{2}\sigma)}]\frac{e^{-\pi/4}}{\sqrt{2}}. \qquad (31a)$$

For $\delta w/\delta T < 0$, $(w_{vb})_{max}$ changes sign from negative to positive at $\tau = \tau_c$, where

$$\tau_c = \sqrt{2}\sigma \ln\left(1 - \frac{1}{\sqrt{2}(\delta w/\delta T)}\right). \qquad (31b)$$

It is obvious in (31*a*) and (31*b*) that, in the vertical boundary layer, motions are downward for $0 \leqslant \tau < \tau_c$, and upward for $\tau > \tau_c$. For example, for $\sigma = 1.0$, $\delta w = 1.0$ and $\delta T = -2.0$ we have $\tau_c \approx 1.3$, which is consistent with the computed data in figure 11.

From (31*b*), the characteristic timescale τ_c is estimated for two limiting cases:

(*a*) if $\delta w/\delta T \to -\infty$, i.e. δw is fixed and $\delta T \to 0^-$, $\tau_c \to 0$;

(*b*) if $\delta w/\delta T \to 0$, i.e. $\delta w \to 0^+$ and δT is fixed, $\tau_c \to \infty$.

In effect, (*a*) refers to the stratifying process induced by a throughflow with no thermal loading at the vertical wall. In this case, there is no recirculating flow in the interior to begin with. Problem (*b*) represents the stratifying process initiated by a thermal loading at the vertical wall with no throughflow. As documented for this case, over the heat-up timescale, the recirculating flow in the global region controls the overall cool-down process. The qualitative interpretations of these two limiting cases involving τ_c are in line with the physical depictions of the overall transient adjustment process.

6. Comparisons of numerical and theoretical solutions

A full numerical solution to the governing equations is obtained to validate the major assertions of the theoretical analysis. Specifically, numerical computational results for the configuration $\delta w \delta T < 0$ of § 5 will be scrutinized.

The complete non-dimensionalized Navier–Stokes equations are

$$\frac{\partial u}{\partial x} + \frac{\partial w}{\partial z} = 0,$$

$$\frac{\partial u}{\partial t} + \epsilon\frac{\partial (uu)}{\partial x} + \epsilon\frac{\partial (wu)}{\partial z} = -\frac{\partial p}{\partial x} + Ra^{-1/2}\left(\frac{\partial^2 u}{\partial x^2} + \frac{\partial^2 u}{\partial z^2}\right),$$

$$\frac{\partial w}{\partial t} + \epsilon\frac{\partial (uw)}{\partial x} + \varepsilon - \frac{\partial (ww)}{\partial z} = -\frac{\partial p}{\partial z} + T + Ra^{-1/2}\left(\frac{\partial^2 w}{\partial x^2} + \frac{\partial^2 w}{\partial z^2}\right),$$

$$\sigma\frac{\partial T}{\partial t} + \epsilon\frac{\partial (uT)}{\partial x} + \epsilon\frac{\partial (wT)}{\partial z} + w = Ra^{-1/2}\left(\frac{\partial^2 T}{\partial x^2} + \frac{\partial^2 T}{\partial z^2}\right).$$

Again, the above system is characterized by the Prandtl number $\sigma = \mu_0^* C_{p0}^*/k_0^*$ the Rayleigh number $Ra = \rho_0^{*2} g^* L^{*3} \beta_0^* \Delta T^* C_{p0}^*/k_0^* \mu_0^*$ and the Rossby number ϵ which measures the strength of nonlinear effects stemming from the external disturbance.

For the numerical solution, the parameter values are chosen to be compatible with the previous linear theoretical analysis, i.e. $\sigma = 1.0$, $Ra = 10^7$, $\epsilon = 0.01$, $\delta w = 1.0$, $\delta T = -2.0$, to simulate a cooperating configuration ($\delta w \delta T < 0$).

For the numerical computation, the initial and boundary conditions are

$$u = w = T = 0 \quad \text{at} \quad t = 0,$$

and

$$u = w = 0, \quad T = \delta T = -2.0 \quad \text{at} \quad x = \pm 1.0,$$

$$u = 0, \quad w = Ra^{-1/4}\delta w = 10^{-7/4} \quad \text{at} \quad z = \pm 1.0.$$

The numerical computations were performed using the EL2D code, which is based on the SIMPLER algorithm (Patankar 1980). A staggered and stretched grid, with 81×81 mesh points, was deployed. A large number of grid- and time step-convergence tests were conducted, and the outcome was satisfactory. The details of the numerical computations have been well documented (Patankar 1980).

The results of numerical solution are displayed in figures 12–14. The time-dependent evolution of the stream function is shown in figure 12, which is in accord with the results of § 5. At early times, near the vertical sidewall, due to $\delta T < 0$, downward motions are seen (see figure 12*a*). This creates a strong clockwise circulation. At later times, as cool-down in the interior progresses, the clockwise circulation weakens (see

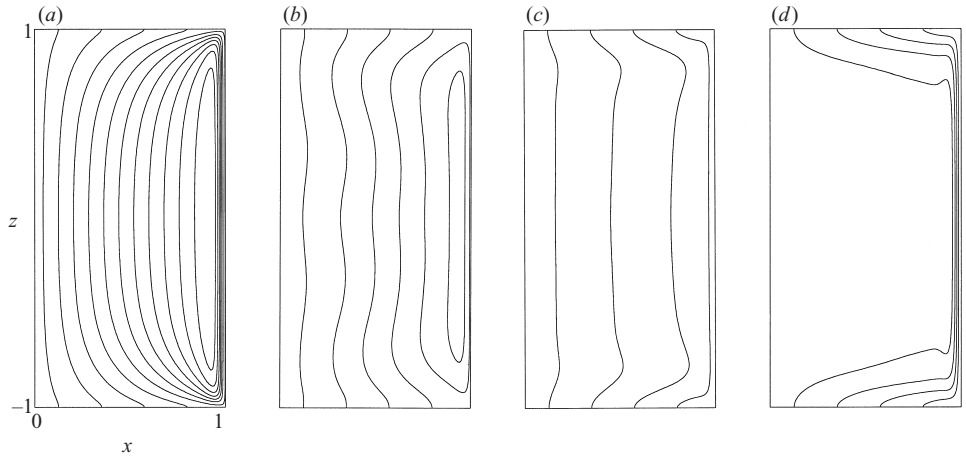

FIGURE 12. Results of the full numerical solution. Plots of stream function (Ψ) for the buoyant-convection-dominant mode ($\delta w = 1.0$, $\delta T = -2.0$). Times, τ, are: (*a*) 4.22×10^{-2}; (*b*) 7.6×10^{-1}; (*c*) 1.69; (*d*) 16.9. $\sigma = 1.0$ and $Ra = 10^7$. $\Delta\Psi = 0.0035$.

figure 12*b*). At still later times, the overall flow is controlled by the forced-convection mode of the opposing configuration (see figure 12*c*, *d*).

Note the weak waviness seen in the streamline pattern at intermediate times in figure 12(*b*). This reflects the presence of inertial oscillation, which is characterized by the Brunt–Väisälä frequency $N = (\beta_0^* \Delta T^* g^* / L^*)^{1/2}$ stemming from the basic stratification. Recall that the foregoing theoretical analysis was carried out by using the heat-up timescale $[O(N^{-1}Ra^{1/4})]$, which is much larger than the inertial oscillation timescale $[O(N^{-1})]$. Therefore, the theoretical predictions do not capture the weak wavy patterns in the streamlines in the interior. The general flow patterns of the theoretical analysis of § 5, viewed over the whole heat-up process, are clearly in line with the numerical solution. Close agreement is seen between the theoretical and numerical solutions for the temperature field, as shown in figure 13. It also shows the progress of cool-down in the interior.

The time history of the vertical velocity (w) near the vertical boundary layer is plotted in figure 14. Good agreement is apparent between the theoretical and numerical solutions. However, it is noted that, at the initial state ($\tau \to 0$), the numerical solution shows $w \to 0$, whereas $w \neq 0$ in the theoretical solution. This is again explained by the fact that, in the theory, time is scaled by the heat-up timescale $[O(N^{-1}Ra^{-1/4})]$, which is much larger than the timescale of formation of the vertical boundary layer $[O(N^{-1})]$. Consequently, in the theory, at the initial state ($\tau \to 0$), the vertical boundary layer has already been established. This discrepancy, however, does not invalidate the usefulness of the overall analysis of the heat-up process. Note also that the results in figure 14 corroborate the definition for τ_c($\tau_c \approx 1.3$ based on (31*b*)), which indicates the timescale over which the clockwise circulation flow near the sidewall vanishes. In summary, the principal assertions of the present theoretical developments are shown to be highly consistent with the full numerical solutions.

7. Concluding remarks

The transient processes of an initially stationary and stably stratified fluid in a square container is studied by employing the matched asymptotic method. The

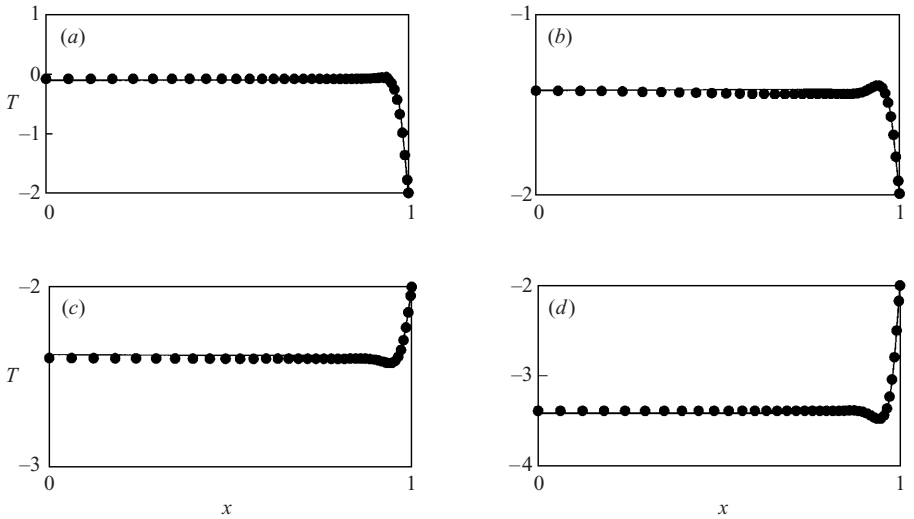

FIGURE 13. Profiles of temperature, T, fields at $z = 0$ ($\delta w = 1.0$, $\delta T = -2.0$). Times, τ, are: (*a*) 4.22×10^{-2}; (*b*) 7.6×10^{-1}; (*c*) 1.69; (*d*)16.9. $\sigma = 1.0$ and $Ra = 10^7$. ——, theory; ●, numerical solution.

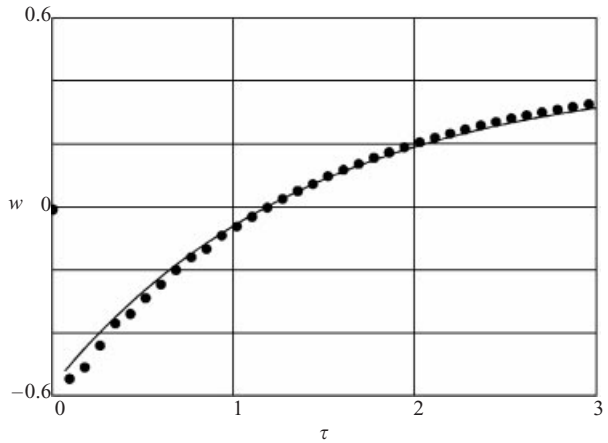

FIGURE 14. Times histories of vertical velocity, w, at $x = 0.974$ and $z = 0$ ($\delta w = 1.0$, $\delta T = -2.0$). $\sigma = 1.0$ and $Ra = 10^7$. ——, theory; ●, numerical solution.

boundary walls are highly conducting. Flow is induced by the simultaneous switch-on of a temperature increase (δT) at the vertical wall and a vertical throughflow ($Ra^{-1/4}\delta w$) at the horizontal walls.

The transient adjustment in the interior over the heat-up timescale, $t \sim O(Ra^{1/4})$, is mainly effected by the vertical motions of magnitude $O(Ra^{-1/4})$. The horizontal boundary layer is of double-layered structure: an $O(Ra^{-1/8})$ outer layer and an $O(Ra^{-1/6})$ inner layer. The transient outer layer matches the flow features between interior and boundary layers. The steady inner layer satisfies the no-slip condition at the horizontal walls. The vertical boundary layer is formed over $t \sim O(1)$, and it exhibits the characteristics of a buoyancy layer.

The explicit character of the transient flow is determined by $\delta w/\delta T$, and opposing ($\delta w/\delta T > 0$) and cooperating ($\delta w/\delta T < 0$) configurations are considered.

In the opposing configurations, $\delta w/\delta T$ represents a mixed convection parameter. The overall flow pattern may be characterized as (i) a forced-convection-dominant mode ($\delta w/\delta T > 1/\sqrt{2}$), (ii) a buoyancy-convection-dominant mode ($0 < \delta w/\delta T < 1/\sqrt{2}$), (iii) a static mode ($\delta w/\delta T \approx 1/\sqrt{2}$).

In the forced-convection mode ($\delta w/\delta T > 1/\sqrt{2}$), in the transient phase the vertical boundary layer cannot accommodate the entire fluid transport of the throughflow. In the interior, therefore, cool-down occurs due to the upward motion of cold fluid from below. At large times, the vertical boundary layer is strengthened to carry more fluid. In the steady state, the interior motions subside and a new equilibrium state is reached.

In the buoyant-convection-dominant mode ($0 < \delta w/\delta T < 1/\sqrt{2}$), in the transient phase the fluid transport in the vertical boundary layer is larger than the throughflow. Therefore, part of the fluid is returned to the interior near the top horizontal wall. This causes downward motion of hot fluid from above, and the interior heats up. At large times, the vertical boundary layer weakens, and a new equilibrium state is approached.

The static mode ($\delta w/\delta T \approx 1/\sqrt{2}$) is a special case of the opposing configuration. The fluid transport in the vertical boundary layer balances the throughflow at the bottom horizontal wall. The transient characteristics are visible only in the horizontal boundary layer, and the other regions are essentially steady over the heat-up timescale.

In the cooperating configuration ($\delta w > 0$, $\delta T < 0$), sinking motions occur in the vertical boundary layer at small times, which produces a clockwise-circulation flow in the interior ($0 < x < 1$). The throughflow near the bottom horizontal wall is pushed toward the cavity centreline ($x = 0$), and the throughflow is transported directly via the interior toward the top horizontal wall. As cool-down in the interior progresses, the interior temperature becomes lower than that of the vertical wall, so that rising motions occur in the vertical boundary layer. This switch-over time τ_c is computed, and for $\tau > \tau_c$ the general flow pattern is similar to that of the forced-convection-dominant mode.

This work was supported by grants from the NRL-Project, MOST, KOSEF, South Korea.

REFERENCES

Barcilon, V. 1968 Stewartson layers in transient rotating fluid flows. *J. Fluid Mech.* **33**, 815–825.

Batchelor, G. K. 1954 Heat transfer by free convection across a closed cavity between vertical boundaries at different temperature. *Q. Appl. Maths* **12**, 209–233.

Bergholz, R. F. 1978 Instability of steady natural convection in a vertical fluid layer. *J. Fluid Mech.* **84**, 743–768.

Elder, J. W. 1965 Laminar free convection in a vertical slot. *J. Fluid Mech.* **23**, 77–98.

Gill, A. E. 1966 The boundary layer regime for convection in a rectangular cavity. *J. Fluid Mech.* **26**, 515–536.

Greenspan, H. P. 1968 *The Theory of Rotating Fluids*. Cambridge University Press.

Heijst, G. J. F. van 1982 The shear layer structure in a rotating fluid near a differentially rotating sidewall. *J. Fluid Mech.* **130**, 1–12.

Hunter, C. 1967 The axisymmetric flow in a rotating annulus due to a horizontally applied temperature gradient. *J. Fluid Mech.* **27**, 753–778.

Hyun, J. M. 1984 Transient process of thermally stratifying an initially homogeneous fluid in an enclosure. *Intl J. Heat Mass Transfer* **27**, 1936–1938.

Hyun, J. M. 1985 Thermally-forced stratification build-up in an initially homogeneous fluid. *J. Phys. Soc. Japan* **54**, 942–949.

HYUN, J. M. 1987 Heat-up of an initially iso-thermal fluid in an enclosure with semi-conducting boundaries. *J. Phys. Soc. Japan* **56**, 942–948.

HYUN, J. M. & HYUN, J. C. 1986 Adjustment of a thermally-stratified fluid in a container with vertical through-flow. *Intl J. Heat Mass Transfer* **29**, 1487–1493.

JISCHKE, M. C. & DOTY, R. T. 1975 Linearized buoyant motion in a closed container. *J. Fluid Mech.* **71**, 729–754.

PARK, J. S. & HYUN, J. M. 1998 Transient behavior of vertical buoyancy layer in a stratified fluid. *Intl J. Heat Mass Transfer* **41**, 4393–4397.

PATANKAR, S. V. 1980 *Numerical Heat Transfer and Fluid Flow*. Hemisphere.

PATTERSON, J. & IMBERGER, J. 1980 Unsteady natural convection in a rectangular cavity. *J. Fluid Mech.* **100**, 65–86.

PHILLIPS, W. F. & DAVE, R. N. 1982 Effects of stratification on the performance of liquid-based solar heating system. *Solar Energy* **29**, 1487–1493.

RAHM, L. 1986 On the thermal adjustment of an almost enclosed region with through-flow. *Intl J. Heat Mass Transfer* **29**, 1479–1485.

RAHM, L. & WALIN, G. 1979*a* Theory and experiments on the control of the stratification in almost-enclosed regions. *J. Fluid Mech.* **90**, 315–325.

RAHM, L. & WALIN, G. 1979*b* On thermal convection in stratified fluids. *Geophys. Astrophys. Fluid Dyn.* **13**, 51–65.

SAKURAI, T. & MATSUDA, T. 1972 A temperature adjustment process in a Boussinesq fluid via a buoyancy-induced meridional circulation. *J. Fluid Mech.* **54**, 417–421.

WALIN, G. 1971 Contained non-homogeneous flow under gravity or how to stratify a fluid in the laboratory. *J. Fluid Mech.* **48**, 647–672.

VERONIS, G. 1970 The analogy between rotating and stratified fluids. *Annu. Rev. Fluid Mech.* **2**, 37–66.